

Peer review status:

This is a non-peer-reviewed preprint submitted to EarthArXiv.

Assessing uncertainty of source rock properties using Monte Carlo basin modeling – Application to Canning Basin, Australia

Jiayuan Huang^{a*}, Tapan Mukerji^{a,b,c}

^a Department of Energy Science & Engineering, Stanford University, Stanford, California, USA

^b Department of Earth & Planetary Sciences, Stanford University, Stanford, California, USA

^c Department of Geophysics, Stanford University, Stanford, California, USA

*jiayuanh@stanford.edu

Abstract

This study presents a Monte Carlo basin modeling framework for quantifying uncertainty in source rock property predictions by integrating geological, geophysical, and geochemical inputs. The approach accounts for variability in petrological parameters from rock physics inversion, paleo-erosion magnitudes, organic facies properties, and boundary conditions to simulate source rock properties such as vitrinite reflectance, transformation ratio, temperature, and pore pressure. Application to the Goldwyer III Formation in the Canning Basin, Australia, reveals that the source rock is within the oil to wet gas window, with substantial but incomplete transformation. Sensitivity analysis identifies Cretaceous erosion and heat flow as the dominant controls on thermal maturity, while the transformation ratio is also strongly influenced by the hydrocarbon generation kinetics model. Comparison with rock physics inversion and T_{\max} -based maturity calculations demonstrates that Monte Carlo basin modeling significantly reduces uncertainty by incorporating geological constraints and process-based modeling. This integrated framework improves the reliability of source rock property assessments and offers a valuable tool for exploration risk reduction.

Keywords: Uncertainty quantification; Monte Carlo simulation; Basin and Petroleum System modeling; Unconventional shale; Thermal maturity; Source rock properties; Canning Basin

1 Introduction

Quantifying the thermal and burial evolution of sedimentary basins is essential for understanding petroleum system development and assessing exploration risk. Rock physics inversion is a powerful tool for estimating subsurface source rock properties from well logs or seismic data. However, key properties such as thermal maturity, transformation ratio, and pore pressure are difficult to infer accurately through rock physics inversion alone. To address this challenge, Basin and petroleum system modeling (BPSM) integrates geological, geochemical, and geophysical data to simulate the processes that control hydrocarbon generation, migration, and accumulation over geological time (Hantschel & Kauerauf, 2009). Despite its strengths, BPSM still relies on numerous input parameters including paleo-heat flow, erosion magnitudes, organic facies properties, and kinetic models that are inherently uncertain due to limited data availability, spatial variability, and interpretational ambiguities.

Traditional basin models are often constructed using deterministic input values, which may oversimplify the range of geological scenarios, lead to misleading predictions of source rock maturity, hydrocarbon generation, and reservoir quality, and may not assess the associated uncertainties of the predictions. Recognizing and quantifying these uncertainties is crucial for making more robust geological interpretations and for guiding exploration decisions (Peters et al., 2012).

Monte Carlo simulation provides a powerful framework for addressing input uncertainties in basin modeling by treating key parameters as probability distributions rather than fixed values. Through stochastic sampling and multiple model realizations, Monte Carlo basin modeling can capture the range of possible geological outcomes and provide probabilistic assessments of thermal histories, hydrocarbon generation timing, and petroleum system efficiency. Brevik et al. (2014) introduced the term geophysical basin modeling (GBM) to describe the process of estimating velocity models by integrating rock physics with basin modeling results. Tong and Mukerji (2017) implemented Monte Carlo basin modeling combined with sensitivity analysis to identify the impact of uncertain parameters on both spatial and temporal model responses. Tømmerås et al. (2018) employed an iterative Monte Carlo basin-modeling workflow that probabilistically calibrates uncertain input parameters by weighting the misfit between observed and modeled oil- and gas-column heights. More recently, Fonseca et al. (2023) proposed Bayesian Geophysical Basin Modeling (BGBM), which integrates geological data, physical modeling, and geologic knowledge through Monte Carlo simulation and Bayesian inference to quantify uncertainty for pore pressure prediction in sedimentary basin models.

In this study, we apply a Monte Carlo-based basin modeling workflow to the Goldwyer III Formation in the Canning Basin, Western Australia to quantify uncertainty for important source rock properties. Key geological uncertainties, including source rock lithology, organic-facies properties, kinetic models, erosion magnitudes, heat flow history, are treated as stochastic variables. A total of 500 basin models were generated using PetroMod, with inputs sampled from defined probability distributions based on well data, geochemical analyses, rock physics inversion, and regional geological interpretations. The simulation results are used to evaluate the range of source rock properties such as hydrocarbon generation potential, temperature, pressure, and associated uncertainties in the Goldwyer III Formation.

In the following sections, Section 2 introduces the geological setting and data in the study area. Section 3 outlines the methodology used in this work. Section 4 presents the basin model input table configuration and defines the prior distributions for the uncertain inputs. Section 5 shows the simulation step. Section 6 reports the results of the Monte Carlo simulations, including sensitivity analysis and an assessment of uncertainty reduction compared to rock physics inversion. Finally, Section 7 provides the discussion and conclusions of the study.

2 Geologic setting and data

This section provides the geological context, data and motivation for basin modeling and maturity analysis. It begins with an overview of the regional geological framework of the Canning Basin, followed by a description of the stratigraphy and key source rock characteristics. The tectonic history and its influence on burial and thermal evolution are then discussed. Finally, we present

the well and seismic data used in this study, along with an assessment of the limitations of rock physics inversion in constraining key thermal maturity indicators.

2.1 Regional geological framework

The Canning Basin, located in northwestern Australia, is one of the largest and least explored sedimentary basins in the region. It is a large Paleozoic basin characterized by a thick and relatively underexplored stratigraphic succession. Deposition within the basin includes major episodes of evaporite formation followed by salt tectonism, an extensive succession of Devonian reef facies, and repeated phases of continental to marine shelf sedimentation in an intracratonic setting (D'Ercole et al., 2003). The Canning Basin hosts multiple proven and potential petroleum systems (Schenk et al., 2018).

2.2 Stratigraphy and source rock characteristics

The study area is in the Broome platform, where the Ordovician Willara, Goldwyer and Nita Formations have good hydrocarbon potential (Figure 1). In this study, we focus on the Goldwyer III Formation which is the primary source rock in this area. The Goldwyer Formation is a Lower to Middle Ordovician organic-rich marine shale deposited in an open marine environment (Cadman et al., 1993; Haines, 2004). It is subdivided into upper shale unit (Goldwyer I), middle carbonate unit (Goldwyer II), and lower shale unit (Goldwyer III) (Foster et al., 1986). The Goldwyer III Formation exhibits high total organic carbon (TOC) and predominantly oil-gas-prone Type II-III and gas-prone Type III kerogen, making it one of the most significant source rocks in the basin (Johnson et al., 2020; Iqbal et al., 2022).

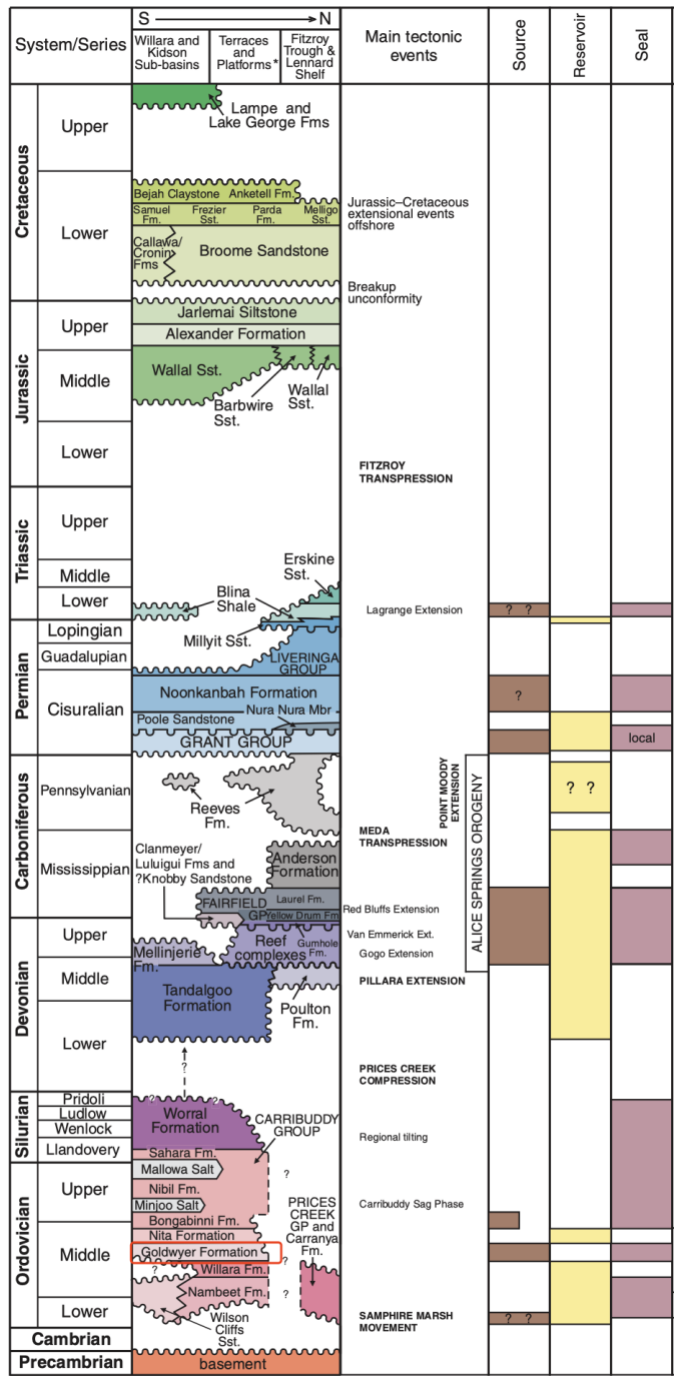


Figure 1. Generalized stratigraphy and main tectonic events of the Canning Basin (Modified from Haines, 2011)

2.3 Tectonic history

The tectonic history of the Canning Basin includes several major events: Samphire Marsh extension (Ordovician–Silurian), Princes Creek compression (Devonian–Carboniferous), Meda transpression (Carboniferous–Triassic), Fitzroy transpression (Triassic–Jurassic), and Jurassic–Cretaceous extension (Ghori et al., 2007; Haines, 2011) (Figure 1). These events created regional

unconformities and significantly influenced the burial and maturity of the Goldwyer III Formation. The tectonic history will be used to reconstruct the basin's thermal history and further constrain the basin modeling.

2.4 Well and seismic data

Theia-1 is the key well in this study. The well penetrates the Goldwyer III Formation (Figure 2) and provides biostratigraphy, geochronology, inorganic and organic geochemistry, petrography, and petrophysics datasets. Additionally, a 2D pre-stack seismic inversion section across the Theia-1 well is available, containing P-wave impedance, density, and V_P/V_S , the ratio of P-to-S-wave velocities.



Figure 2. Locations of well and seismic survey in the Canning Basin. Red dots indicate well location while the blue curve represents the 2-D seismic section.

2.5 Limitations of rock physics inversion in estimating key properties

Statistical rock physics inversion was applied using the seismic data and well log described above to estimate key source rock properties, including vitrinite reflectance, porosity, kerogen, and mineral composition within the Goldwyer III Formation (Huang et al., 2025). While the porosity, kerogen content and clay content were better constrained, the inversion results showed minimal posterior updating of vitrinite reflectance relative to the prior distribution, indicating that elastic properties from seismic data and available well logs provided limited sensitivity to vitrinite reflectance (Figure 3). This outcome reflects a fundamental limitation of rock physics inversion for this case: while effective at constraining elastic and compositional properties, it is generally not well suited for capturing properties primarily governed by burial and thermal history.

To overcome this limitation, we introduce a Monte Carlo basin modeling approach in the following section, which explicitly incorporates geologic processes such as sedimentation, erosion, heat flow, and kerogen kinetics to estimate thermal maturity (vitrinite reflectance) and related outputs probabilistically.

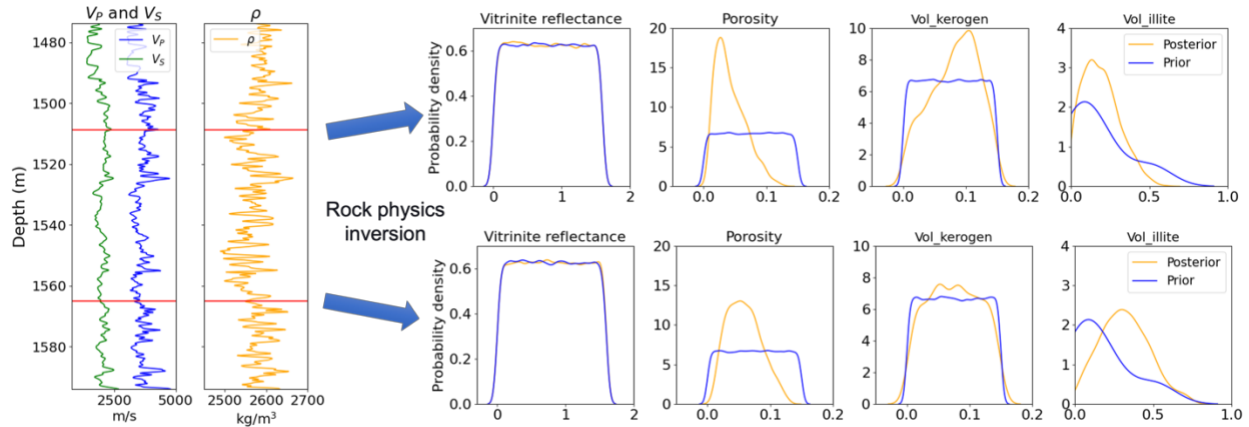


Figure 3. Limitations of rock physics inversion in estimating vitrinite reflectance from elastic properties in the Goldwyer III Formation. While the inversion produces noticeable updates in the posterior distributions of porosity, kerogen content, and mineral compositions, it fails to constrain vitrinite reflectance, which remains nearly identical to the prior distribution (Huang et al., 2025).

3. Methods

This section introduces the methodology used to model the burial, thermal, and hydrocarbon generation history of the Goldwyer III Formation. Basin modeling requires a range of geological and geophysical inputs, including stratigraphy, lithology, paleo-water depth, heat flow history, erosion events, and geochemical parameters such as hydrogen index (HI) and kerogen kinetics. These inputs are derived from the rock physics inversion, well logs, stratigraphic interpretations, and tectonic history introduced in Section 2, and are integrated into a Monte Carlo framework to quantify uncertainty and explore the range of possible source rock properties that cannot be reliably constrained through rock physics inversion alone.

3.1 Proposed workflow

In this study, Monte Carlo basin modeling is applied to estimate source rock properties that cannot be directly inferred from rock physics inversion using elastic properties derived from well logs and seismic data (Figure 4). The posterior distributions of key source rock properties, including kerogen content, porosity, and mineral compositions, are randomly sampled to construct the source rock formation input for basin modeling. Well logs are utilized to estimate paleo-erosion and infer kinetics and the hydrogen index (HI) of the organic facies. Boundary conditions, such as paleo water depth (PWD), sediment-water interface temperature (SWIT), and heat flow (HF), are constrained using biostratigraphy and regional tectonic history. Multiple realizations of basin models are then generated and used in the simulations. The Monte Carlo basin modeling outputs include thermal maturity ($\%R_o$), temperature, transformation ratio (TR), fluid saturation, permeability, and pressure, providing insights into the uncertainties associated with the source rock system.

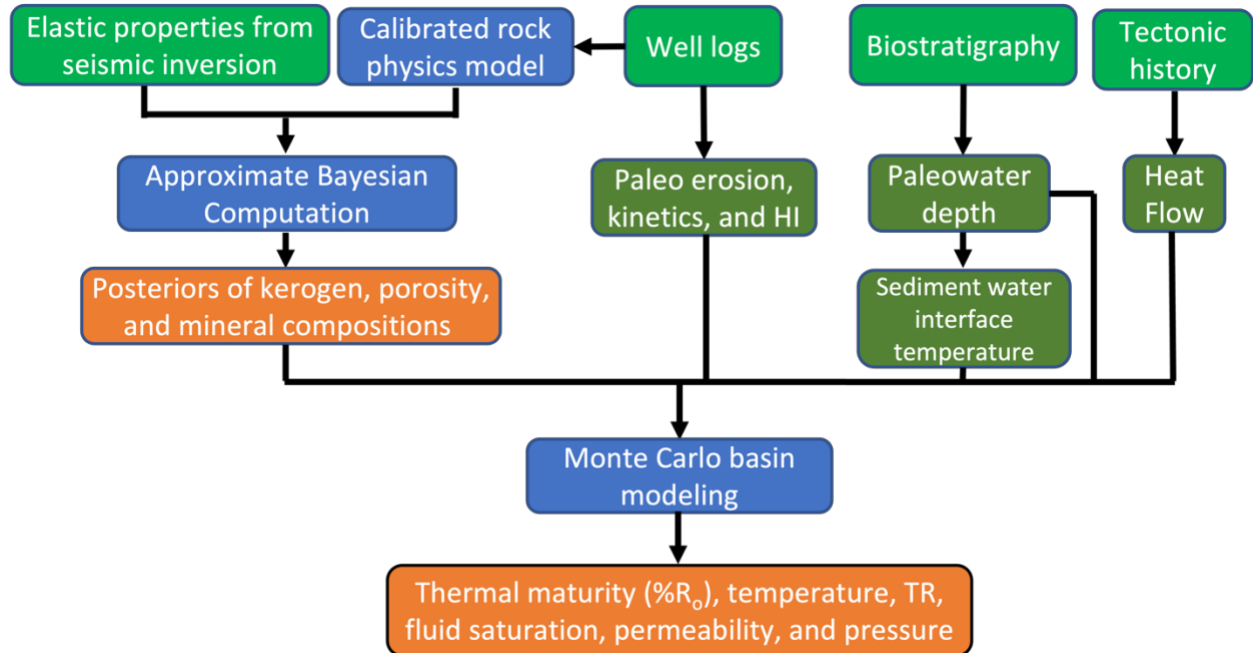


Figure 4. Proposed workflow of Monte Carlo basin modeling. TR is transformation ratio; HI is hydrogen index.

3.2 Monte Carlo basin modeling

The Stanford Basin and Petroleum System Modeling PetroMod Toolbox for MATLAB is used to automate multi-model construction and simulation (Al Ibrahim, 2019) in the commercial PetroMod basin modeling software. The workflow of the toolbox is as follows (Figure 5):

1. Build a template model using the PetroMod graphical user interface (GUI).
2. Define parameters (e.g., lithology, hydrogen index (HI), boundary conditions, etc.) and their probability distributions for Monte Carlo sampling.
3. Generate multiple basin models by duplicating the template and modifying its parameters based on Monte Carlo samples.
4. Execute simulations for all the basin models.
5. Load the simulation results from all the models.
6. Analyze the simulated results for further interpretation.

Steps 3, 4, and 5 are independent for each model, allowing them to be executed in parallel to significantly reduce computational time.

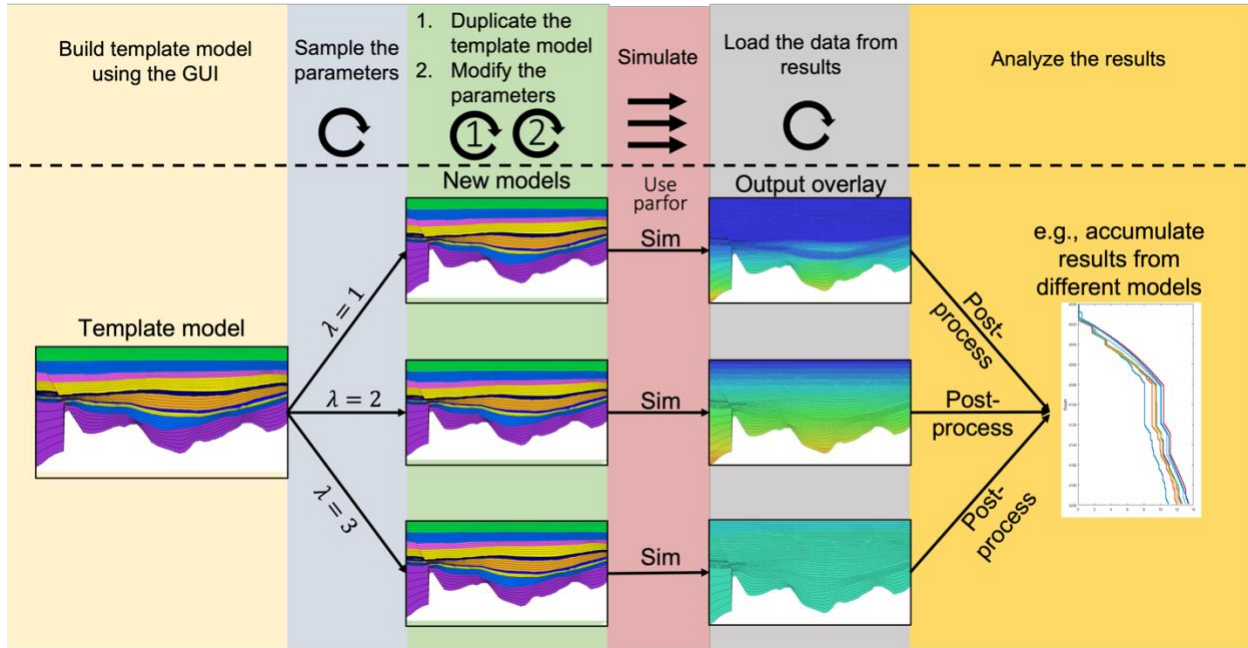


Figure 5. Workflow for the Stanford BPSM PetroMod Toolbox for MATLAB (modified from Al Ibrahim, 2019).

4. Monte Carlo basin modeling inputs

This section outlines the input parameters and uncertainties considered in the Monte Carlo basin modeling framework. It begins with the 1D basin model template and then details the estimation of key uncertain parameters, including petrological properties, paleo-erosion magnitudes, organic facies characteristics, and boundary conditions. Finally, a summary of the Monte Carlo sampling strategy is provided.

4.1 Input table of 1D basin model template

In this study, a 1D basin model template serves as the foundational structure for Monte Carlo basin modeling. The input table of the template provides the fundamental geological, geochemical, and thermal properties required for basin modeling. These values act as baseline inputs for the simulation and include formation depths, ages, erosion estimates, organic facies properties, and thermal boundary conditions. The input table consolidates data from well logs, seismic inversion, geochemical analysis, and regional geological studies, ensuring a realistic representation of the subsurface system.

Monte Carlo simulations are then applied by randomly sampling uncertain parameters, duplicating the template models, and replacing the corresponding values in each duplicated template model. This process generates multiple realizations of the basin model, allowing for a comprehensive uncertainty analysis of key basin parameters, such as thermal history and hydrocarbon generation potential.

A basin model template used in this study is prepared based on the stratigraphy in Figure 1 and is shown in Table 1.

Age (Ma)	Formation	Depth (m)	Thickness (m)	Event type	Paleodeposition/ Erosion (m)	Lithology	PSE	Kinetic	TOC (wt. %)	HI (mg/g TOC)
0	Recent	0	10	Deposition		Sandstone (typical)	Overburden Rock			
70	Broome Sandstone	10	30	Deposition		Sandstone (typical)				
100	Cretaceous Erosion	40	0	Erosion	Erosion 1					
150	Jarlemat Siltstone	40	125	Deposition	Deposition 1	Siltstone (organic lean)				
165	Wallal Sandstone	165	76	Deposition		Sandstone (typical)	Reservoir Rock			
250	Lower Triassic Erosion	241	0	Erosion	Erosion 2					
280	Grant Formation	241	600	Deposition	Deposition 2	Sandstone (typical)				
360	Hiatus L. Devonian	841	0	Hiatus						
436	Carribudy Formation	841	137	Deposition		Shale (typical)	Overburden Rock			
450	Bongabinni Formation	978	41	Deposition		Dolomite (typical)	Seal Rock			
455	Nita Formation	1019	169	Deposition		Siltstone (organic lean)	Reservoir Rock			
463	Goldwyer I	1188	178	Deposition		Shale (organic rich, 3% TOC)	Source Rock	Pepper&Corvi(1995) TII(B)	4	700
465	Goldwyer II	1366	106	Deposition		Limestone (organic rich - typical)				
475	Goldwyer III 1	1472	7	Deposition		Lithology 1	Source Rock	Kinetic 1	TOC 1	HI 1
475.29	Goldwyer III 2	1479	7	Deposition		Lithology 2	Source Rock	Kinetic 2	TOC 2	HI 2
475.59	Goldwyer III 3	1486	7	Deposition		Lithology 3	Source Rock	Kinetic 3	TOC 3	HI 3
475.88	Goldwyer III 4	1493	7	Deposition		Lithology 4	Source Rock	Kinetic 4	TOC 4	HI 4
476.18	Goldwyer III 5	1500	7	Deposition		Lithology 5	Source Rock	Kinetic 5	TOC 5	HI 5
476.47	Goldwyer III 6	1507	7	Deposition		Lithology 6	Source Rock	Kinetic 6	TOC 6	HI 6
476.76	Goldwyer III 7	1514	7	Deposition		Lithology 7	Source Rock	Kinetic 7	TOC 7	HI 7
477.06	Goldwyer III 8	1521	7	Deposition		Lithology 8	Source Rock	Kinetic 8	TOC 8	HI 8
477.35	Goldwyer III 9	1528	7	Deposition		Lithology 9	Source Rock	Kinetic 9	TOC 9	HI 9
477.65	Goldwyer III 10	1535	7	Deposition		Lithology 10	Source Rock	Kinetic 10	TOC 10	HI 10
477.94	Goldwyer III 11	1542	7	Deposition		Lithology 11	Source Rock	Kinetic 11	TOC 11	HI 11
478.24	Goldwyer III 12	1549	7	Deposition		Lithology 12	Source Rock	Kinetic 12	TOC 12	HI 12
478.53	Goldwyer III 13	1556	7	Deposition		Lithology 13	Source Rock	Kinetic 13	TOC 13	HI 13
478.82	Goldwyer III 14	1563	7	Deposition		Lithology 14	Source Rock	Kinetic 14	TOC 14	HI 14
479.12	Goldwyer III 15	1570	7	Deposition		Lithology 15	Source Rock	Kinetic 15	TOC 15	HI 15
479.41	Goldwyer III 16	1577	7	Deposition		Lithology 16	Source Rock	Kinetic 16	TOC 16	HI 16
479.71	Goldwyer III 17	1584	9	Deposition		Lithology 17	Source Rock	Kinetic 17	TOC 17	HI 17
480	Willara Formation	1593	53	Deposition		Limestone (shaly)				
489	Nambeet Formation	1646								

Table 1. 1D basin model template. The variables with green color will be sampled during the Monte Carlo simulation (Modified from Johnson et al., 2020).

4.2 Key uncertain parameters and their estimation

This subsection describes the primary sources of uncertainty in the basin model and the methods used to estimate the distributions of the uncertain parameters. These include petrological inputs derived from rock physics inversion, paleo-erosion estimates, organic facies properties, and boundary condition.

Paleo-erosion plays a critical role in basin modeling by influencing the burial history, thermal evolution, and maturation of source rocks. Significant erosion events can remove substantial overburden, thereby reducing the burial depth and altering the thermal regime of the basin over time (Allen and Allen, 2013). Accurately estimating the magnitude and timing of these erosion events is essential for reconstructing realistic burial and temperature histories.

Organic facies properties are essential inputs for basin modeling, as they govern the timing, quantity, and type of hydrocarbon generation during the thermal evolution of a source rock (Peters and Cassa, 1994). Key properties include hydrogen index (HI), kerogen type, and hydrocarbon generation kinetic model (e.g., activation energy and frequency factor), all of which influence the transformation of organic matter into hydrocarbons under varying burial and thermal conditions.

Basin modeling requires thermal boundary conditions at both the top and base of the sedimentary column. The top thermal boundary condition is the paleosurface temperature, estimated based on paleolatitudes and paleo water depth (PWD) through geologic time (Hsu and Robinson, 2017). In the simulation software, this paleosurface temperature is referred to as the sediment-water interface temperature (SWIT).

4.2.1 Petrological inputs estimated from rock physics inversion

Distributions of petrological inputs including lithology, porosity, and TOC are estimated using the statistical rock physics inversion method from Huang et al. (2025). In this study, a 1D vertical column is extracted from the 2D inversion results. This column, located within the Goldwyer III Formation, is discretized into N layers (with $N = 17$ near the Theia-1 well). At each layer, porosity values are randomly sampled and used to approximate Athy's compaction factor (Athy, 1930) for modeling mechanical compaction. Total organic carbon (TOC) values are resampled from the posterior distribution of kerogen volume fractions obtained through rock physics inversion and converted to weight percent by dividing by two, assuming a kerogen-to-bulk rock density ratio of approximately 1:2 (i.e. assuming kerogen density $\approx 1.3 \text{ g/cm}^3$ (Al Ibrahim, 2019) and bulk rock density $\approx 2.6 \text{ g/cm}^3$). Six mineral components from rock physics inversion—quartz, calcite, illite, chlorite, dolomite, and pyrite—are randomly sampled from their respective posterior distributions. Lithology is then represented by these six minerals using the mixing function in the Lithology Editor of PetroMod. The workflow is shown in Figure 6.

The distributions of porosity and TOC are modeled using kernel density estimation (KDE) based on the posterior samples obtained from the rock physics inversion, while the distributions of mineral compositions are modeled using Dirichlet distributions to ensure that the sampled fractions sum to one (MacKay, 2003). The Dirichlet parameters are estimated via maximum likelihood based on the inversion results (Minka, 2000).

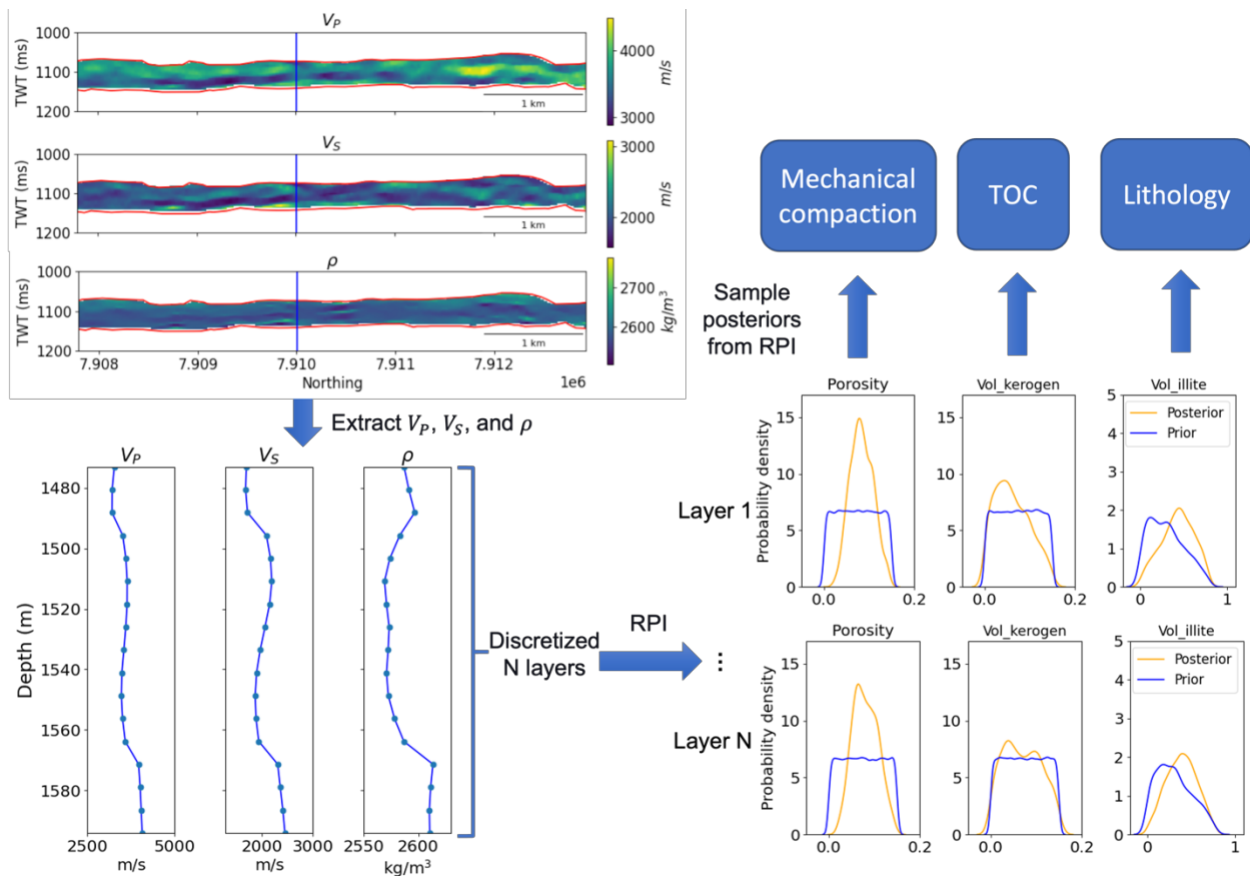


Figure 6. Workflow for sampling posterior distributions from rock physics inversion results to estimate mechanical compaction and petrological inputs for the basin model. RPI is rock physics inversion. TOC is total organic carbon.

4.2.2 Paleo-erosion estimates

Johnson et al. (2017) estimated erosion magnitude using sonic transit time data and erosion magnitudes at eight wells were estimated, as listed in Table 2. The erosion magnitude at the Theia-1 well was approximated using linear interpolation based on the nearby four well data in the study area which is in Table 2.

Well Name	Sections	
	Jurassic-Cretaceous (m)	Carboniferous-Permian (m)
Hilltop-1	400-2100 (1600)	500-2000 (1400)
Aquila-1	800-1900 (1400)	500-2200 (1300)
McLarty-1	200-1200 (800)	1000-2000 (1700)
Kunzea-1	400-800 (500)	200-1800 (900)
Musca-1	600-2000 (1200)	300-1500 (1200)
Matches Springs-1	400-1300 (1000)	300-900 (600)
Santalum-1	900-2000 (1800)	No Records
Edgar Range-1	300-2100 (1000)	200-1700 (1400)
Theia-1 (Estimated)	450-2046 (1109)	267-1706 (1330)

Table 2. Estimation of erosion from Broom Platform wells (Johnson et al., 2019). The values are lower 95% confidence limit, upper 95% confidence limit, and maximum likelihood estimate, respectively. The first eight wells are from Johnson et al. (2019). The highlighted four wells are used for estimating the erosion of Theia-1 well.

The distributions of paleo-erosion magnitudes at the Theia-1 well during the Jurassic-Cretaceous and Carboniferous-Permian periods are approximately modeled using truncated normal distributions, based on the lower 95% confidence limit, upper 95% confidence limit, and maximum likelihood estimate which is shown in Figure 7 (Virtanen et al., 2020).

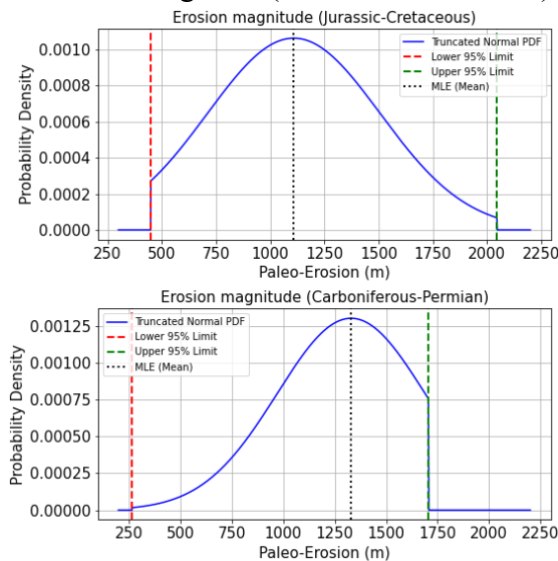


Figure 7. Truncated normal distributions of erosion magnitude during Jurassic-Cretaceous and Carboniferous-Permian.

4.2.3 Organic facies properties

In this study, we compiled Rock-Eval pyrolysis data from the Theia-1 well, including HI and kerogen type, from Johnson et al. (2020) and Iqbal et al. (2022). The HI values range from 60 to 268 mg HC/g TOC, and the distribution is modeled using KDE. Kerogen within the Goldwyer III Formation is classified primarily as Type II and Type II-III, with minor occurrences of Type III. Johnson et al. (2020) demonstrated that the Pepper and Corvi (1995) default kinetics for Type II kerogen in PetroMod most closely match the experimental kinetic results for Type II to II/III within the Goldwyer III Formation. Therefore, for modeling purposes, we randomly sample kinetic models from the PetroMod default Type II kinetics for Type II and Type II-III kerogen, and from the Type III default kinetics for samples classified as Type III (Pepper & Corvi, 1995).

The distribution of kinetic models within the Goldwyer III Formation is constructed and sampled using a Discrete-Time Markov Chain (DTMC; Norris, 1998) to account for spatial correlation and transition dependencies between adjacent layers. Without DTMC, kinetic model assignments would rely on independent random sampling, ignoring geological continuity and potentially producing unrealistic vertical heterogeneity. DTMC allows us to model the likelihood that a given layer's kinetics resemble those of adjacent layers, reflecting stratigraphic trends and improving

geologic realism in the generated realizations. The transition probability matrix is estimated by computing empirical frequencies of kinetic model transitions observed in well log interpretations across the formation and is summarized in Table 3. The actual data histogram and modeled distribution of Hydrogen Index (HI) using KDE based on the available HI dataset are shown in Figure 8.

	Type II-III	Type III
Type II-III	0.9	0.1
Type III	0.1	0.9

Table 3. Transition probability matrix used in the DTMC model to represent the spatial distribution of kerogen types within the formation.

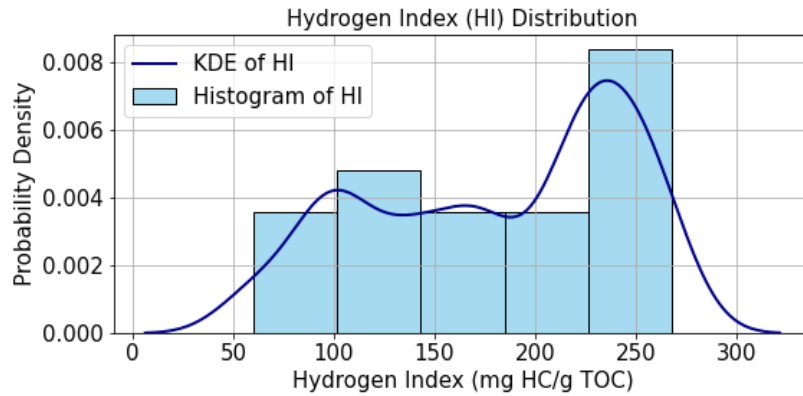


Figure 8. Data histogram and estimated distribution of Hydrogen Index (HI) from Rock-Eval pyrolysis data using KDE.

4.2.4 Boundary conditions

The basal thermal boundary condition is the paleo heat flow (HF), which is one of the most critical input parameters in basin modeling due to its significant impact on the amount, composition, and rate of petroleum generation (Hsu and Robinson, 2017).

In this study, paleo water depths (PWD) are estimated based on the depositional environment reported in the Western Australian Petroleum and Geothermal Information Management System (WAPIMS) biostratigraphy database (Young et al., 2021; Tipsword et al., 1966). The minimum and maximum PWD through geological time in the Canning Basin are shown in Figure 9.

The SWIT values are then calculated using the automatic SWIT tool in PetroMod, which derives values based on PWD and the well location (Wygrala, 1989). The minimum and maximum SWIT through geological time at the well location is presented in Figure 9.

The ranges of HF at different geological times are estimated based on the tectonic history, using typical heat flow values reported by Allen and Allen (2005). A summary of the tectonic history is provided in Table 4, while the estimated HF ranges over time are illustrated in Figure 9.

Boundary conditions are sampled only at the time points where depositional environment and tectonic event data are available. These are assumed to follow a uniform distribution.

Age	Tectonic Event
Late Cretaceous-Present Day	Tectonic quiescence
Early Cretaceous	Tectonic quiescence
End Jurassic	Regional uplift
Middle Jurassic	Tectonic quiescence and thermal subsidence
Middle Triassic-Middle Jurassic	Transgression
Early Triassic	Minor extension
Mid-Late Permian	End of glaciation
Early Permian	Major extension, rifting and subsidence
Early-Late Carboniferous	Alice Springs Orogeny equivalent
End Devonian	Major extension, rifting and rapid subsidence
Early-Mid Devonian	Continued compression, minor subsidence
End Silurian	Regional compression
Late Ordovician-Early Silurian	Thermal subsidence
Middle Ordovician	Rifting and thermal subsidence
Early Ordovician	NW-SW extension and rapid subsidence
Precambrian	

Table 4. Summary of tectonic history in the Canning Basin (Finder exploration, 2018)

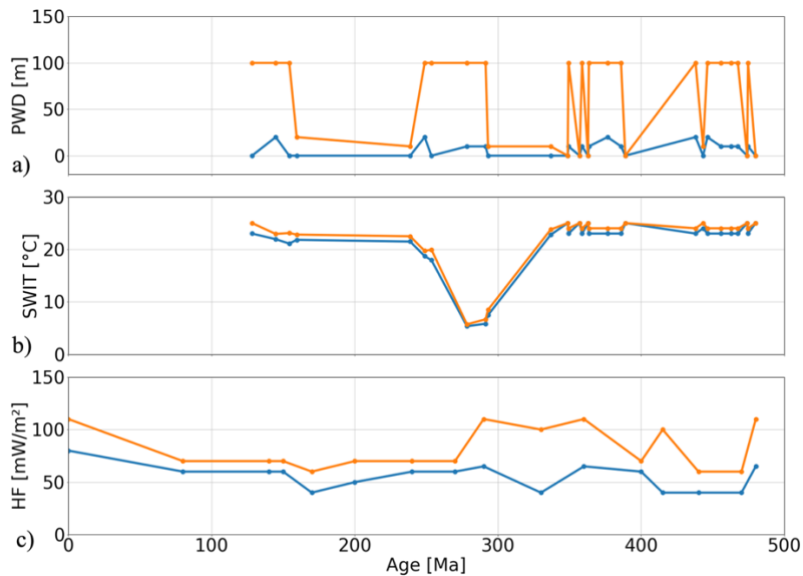


Figure 9. Estimated PWD, SWIT, and HF through geological time (Young et al., 2021; Finder exploration, 2018). The orange and blue curves represent upper and lower bounds respectively. The orange and blue dots are the estimated values based on the depositional environment.

4.3 Summary of Monte Carlo Sampling of uncertain parameters

Some of the uncertain parameters in the basin model are continuous variables, while others are categorical, such as the kinetic model type. For continuous variables, some can be resampled directly from the distributions of existing datasets, whereas others are defined only by estimated value ranges. As a result, different types of variables require different sampling strategies and underlying assumptions.

A summary of all the uncertain parameters, along with their corresponding sampling methods and data sources, is provided in Table 5.

Uncertain parameters	Distribution	Data source
Mineral compositions	Dirichlet distribution	Rock physics inversion
Porosity	KDE	Rock physics inversion
Paleo erosion	Truncated normal distribution	Sonic log
Kinetic model	DTMC	Rock-Eval pyrolysis data
TOC	KDE	Rock physics inversion
HI	KDE	Rock-Eval pyrolysis data
Boundary conditions	Uniform distribution	Depositional environment and tectonic history

Table 5. Summary of all the uncertain parameters and their sampling methods and data sources. KDE is kernel density estimation. DTMC is Discrete-Time Markov Chains.

5 Simulation setup

In the 1D basin model template, simulator options must be configured. Since the template was duplicated with only the input tables and boundary conditions modified, the simulation parameters remain consistent across all realizations. A total of 500 basin models were simulated.

A few simulation parameters were adjusted from their default values: the number of runs was set to 20, the maximum cell thickness to 5 m, and the maximum time step duration to 0.25 Ma. Core measurements show that permeability within the Goldwyer III Formation is in the range of 0.001–0.01 md, and porosity is less than 10%, indicating that the shale is very tight (Finder exploration, 2018). Therefore, it is assumed that generated oil and gas are trapped within the pore system with extremely inefficient expulsion. Accordingly, the simulation was set to "generation only," with an expulsion factor of 10%. "Organic secondary porosity", "Secondary cracking", and "Radiogenic heat" are enabled in the simulation.

Model generation, simulation, and data loading were performed in parallel using a multi-core CPU to improve computational efficiency.

6 Results

This section presents the results of the Monte Carlo basin modeling and associated uncertainty analysis for the Goldwyer III Formation. We first examine the sensitivity of key model outputs to uncertain geological and geochemical inputs. Next, we summarize the distributions of these outputs across all the simulations. Finally, we assess the extent to which Monte Carlo basin

modeling reduces uncertainty in thermal maturity estimates, in comparison to rock physics inversion.

6.1 Sensitivity analysis of the model outputs to the uncertain inputs

In this section, Distance-based generalized sensitivity analysis (DGSA) is applied to evaluate how key uncertain parameters influence model outputs. (Fenwick et al., 2014; Park et al., 2016). The analysis focused on vitrinite reflectance, TR, temperature, and pore pressure within the Goldwyer III Formation.

Since this particular sensitivity analysis algorithm only accepts scalar inputs, depth-varying and time-varying parameters such as porosity, TOC, HI, HF, and PWD are discretized into three representative categories: low, mid, and high, based on evenly divided value ranges. A categorical indicator is then assigned to each realization. For each category, the actual values at each depth or time step are sampled from the corresponding range using a uniform distribution. For input variables such as mineral compositions, which require the component fractions to sum to one, values at each depth are sampled from a Dirichlet distribution. To reduce dimensionality for the sensitivity analysis, the depth-averaged mineral compositions are used as representative scalar inputs. The kinetic model is treated as a categorical input, with a single model assigned uniformly across the full depth for each realization. Erosion magnitudes are directly sampled from their original distributions without further transformation.

This approach allows complex depth- and time-dependent parameters to be incorporated into the sensitivity analysis while preserving key aspects of their variability. A summary of all the input variables and their sampling strategies is listed in Table 6.

Input variable	Type	Sampling method	Value range/ Categories	Notes
Porosity	Depth-varying	Categorical: [Low, Mid, High]	Equal thirds, $p = [1/3, 1/3, 1/3]$	Uniformly sampled within each range at each depth
TOC				
HI				
Mineral Compositions		Dirichlet distribution + Averaging	Posterior from inversion	Averaged across depth
Hydrocarbon generation kinetic Model		Random assignment	[Type II, Type III], $p = [1/2, 1/2]$	One model assigned to full column
Erosions	Scalar	Truncated normal distribution	From erosion maps	Sampled directly from fitted distribution
HF	Time-varying	Categorical: [Low, Mid, High]	Equal thirds, $p = [1/3, 1/3, 1/3]$	Time series simplified using category-based range
PWD				

Table 6. Summary of Input Variables and Sampling Strategies for Sensitivity Analysis.

A total of 500 basin models are simulated. The outputs within the Goldwyer III Formation are extracted and used for sensitivity analysis. The key observations from Figure 10 are summarized below:

- **Vitrinite reflectance:** The most sensitive parameters influencing thermal maturity are Cretaceous erosion and heat flow. Erosion controls the maximum burial depth, and deeper burial typically results in higher temperatures. Therefore, erosion directly affects the peak temperature experienced by the source rock in the past. Earlier erosion (e.g., Triassic) may lead to cooling and reduced maturation rates, as the formation may not reach sufficient burial depth to initiate significant thermal transformation. In contrast, later erosion (e.g., Cretaceous) occurs closer to the time of peak burial and thus has a greater impact on the maximum temperature achieved. Moreover, because vitrinite reflectance is an irreversible maturity indicator, later erosion can preserve the maturity signal even if cooling occurs afterward. As a result, Cretaceous erosion has a stronger influence on maturity than Triassic erosion. Additionally, heat flow directly controls the thermal regime within the basin and significantly affects the temperature evolution of the source rock. In contrast, the hydrocarbon generation kinetic model appears to have limited influence on thermal maturity in this case. This is because vitrinite reflectance is calculated using a separate kinetic model (Sweeney & Burnham, 1990) that primarily depends on maximum temperature and exposure time, rather than the kinetics of hydrocarbon generation.
- **Transformation Ratio (TR):** The transformation ratio (TR) of kerogen is calculated using a hydrocarbon generation kinetic model that assigns different kinetic parameters to different kerogen types and further differentiates between oil and gas generation reactions (Pepper & Corvi, 1995). Therefore, it is reasonable that Cretaceous erosion, kinetic model, and heat flow are the most sensitive factors in the analysis.
- **Temperature:** Heat flow is the only sensitive parameter to impact the current temperature profile. The variation in mineral composition within the Goldwyer III Formation has a minor influence on the source rock temperature. It is because heat primarily propagates upward from the basement in conductive heat transfer. Therefore, only the thermal conductivity of the formation beneath the source rock formation can significantly affect its temperature.
- **Pore pressure:** The top sensitive parameters are porosity, erosion, TOC, and mineral such as quartz and calcite. For porosity, it directly affects pore volume and fluid retention capacity. Erosions influence maximum burial depth and the subsequent exhumation history, which affect compaction trends and pressure buildup. TOC generate hydrocarbons during maturation, contributing to overpressure due to fluid expansion and kerogen-to-hydrocarbon transformation. Quartz and Calcite control the mechanical properties of the rock. Quartz-rich formations are mechanically strong and more resistant to compaction, helping preserve pore space at depth. In contrast, calcite-rich rocks are more ductile and prone to pressure solution, which leads to greater porosity reduction and influences pore pressure buildup.

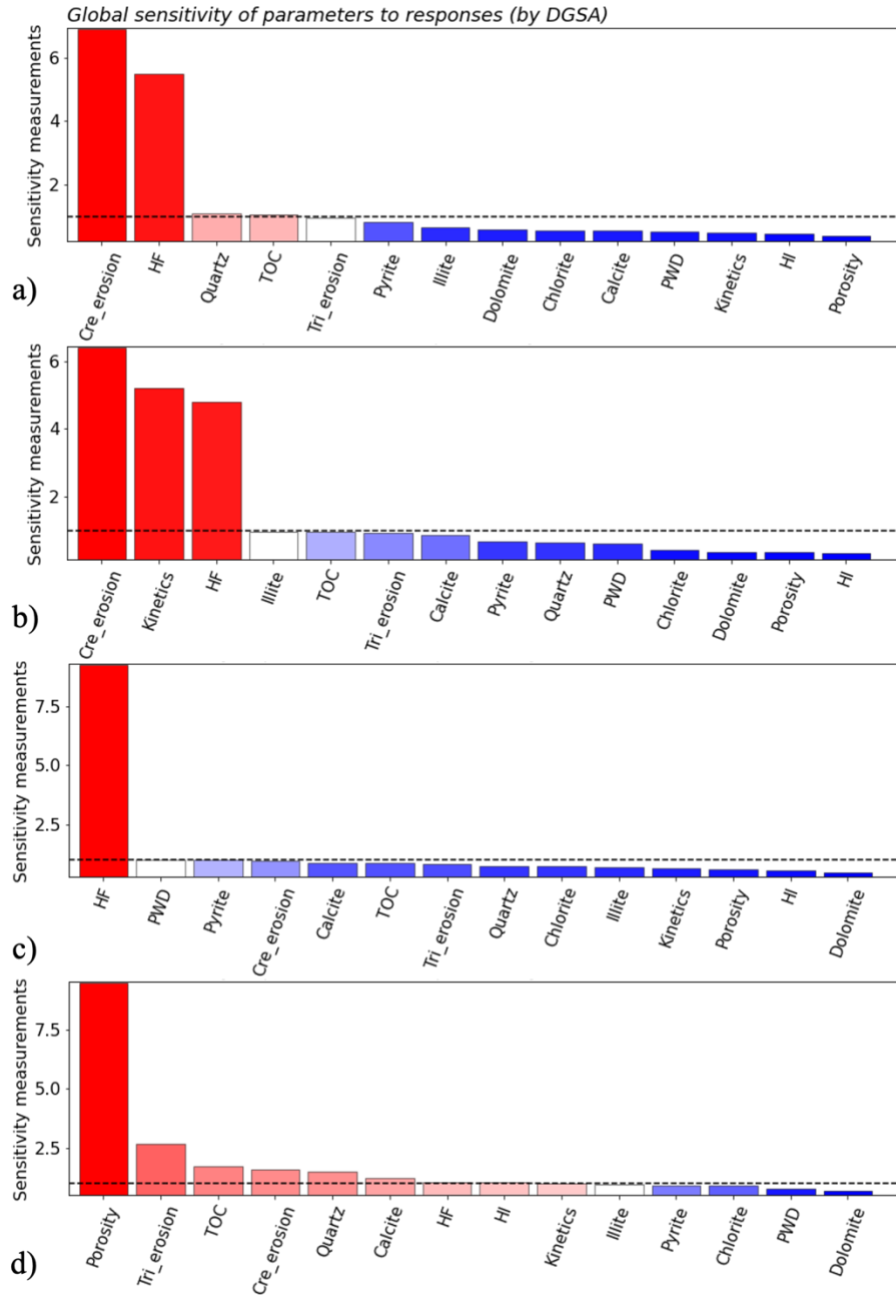


Figure 10. Results of Distance-based Generalized Sensitivity Analysis (DGSA) for key model outputs. Each panel shows the relative importance of uncertain input parameters in influencing the output variable: (a) Vitrinite reflectance, (b) Transformation ratio (TR), (c) Temperature, (d) Pore pressure. Sensitivity is measured using distance-based metrics across categorized input realizations. Bars represent the contribution of each input to output variability. Cre_erosion is Cretaceous erosion. HF is heat flow. TOC is total organic carbon. PWD is paleo water depth. HI is hydrogen index.

6.2 Summary of basin model outputs from Monte Carlo simulation

A new set of 500 basin model realizations was generated for the summary analysis in Section 6.2, independent from the DGSA sample set in Section 6.1. This is because, in Section 6.1, certain depth- and time-dependent input parameters were transformed into scalar or categorical forms to meet the requirements of the DGSA algorithm. As a result, those realizations do not fully preserve the continuous variability of the original inputs. In contrast, the realizations in Section 6.2 were generated using the original, non-discretized input parameter distributions to better capture the full range of model behavior and variability in the Monte Carlo outputs.

Figure 11 shows the depth-dependent distributions of vitrinite reflectance, TR, temperature, and pore pressure. Grey lines represent individual realizations, the red line denotes the median, and the interval between dark blue curves indicates the interquartile range (25th to 75th percentiles). The top and base of the Goldwyer III Formation are shown as light blue and light orange lines, respectively. The key observations are summarized below:

- **Vitrinite reflectance:** Vitrinite reflectance increases with depth across all realizations. Within the Goldwyer III Formation, the vitrinite reflectance range from 0.7 % R_o to 1.5 % R_o , with an interquartile range is between 0.8 % R_o to 1.1 % R_o . These values fall within the oil window (~0.5 % R_o to ~1.0 % R_o) and wet gas window (~1.0 % R_o to ~1.4 % R_o) (Kibria et al., 2020). The uncertainty of vitrinite reflectance widens at greater depths, primarily due to erosion magnitude and thermal boundary condition.
- **Transformation Ratio (TR):** TR increases with depth and shows significant variability within the Goldwyer III Formation. Across all realizations, TR ranges from 10% to 90%, with an interquartile range between 50% and 80%. The median value is approximately 70%, indicating substantial but incomplete transformation across most realizations.
- **Temperature:** Temperature uncertainty increases gradually with depth. The median temperatures at the top and base of the Goldwyer III Formation are approximately 95 °C and 100 °C, respectively. The narrow interquartile range indicate relatively low thermal uncertainty compared to maturity and TR outputs.
- **Pore pressure:** Pore pressure simulations show less variability than other outputs. Above the Goldwyer III Formation, most of the realizations remain near hydrostatic condition. Within the Goldwyer III Formation, the pore pressure shows slightly larger variability, but the interquartile range remains narrow. This is primarily because pore pressure is controlled by the mechanical compaction, permeability, and hydrocarbon generation, while the mechanical compaction and permeability are functions of porosity. In the Monte Carlo sampling, only the porosity within the Goldwyer III Formation is sampled from the inversion.

Overall, vitrinite reflectance and TR exhibit the highest sensitivity to uncertain inputs, while temperature and pore pressure remains less variable across the realizations.

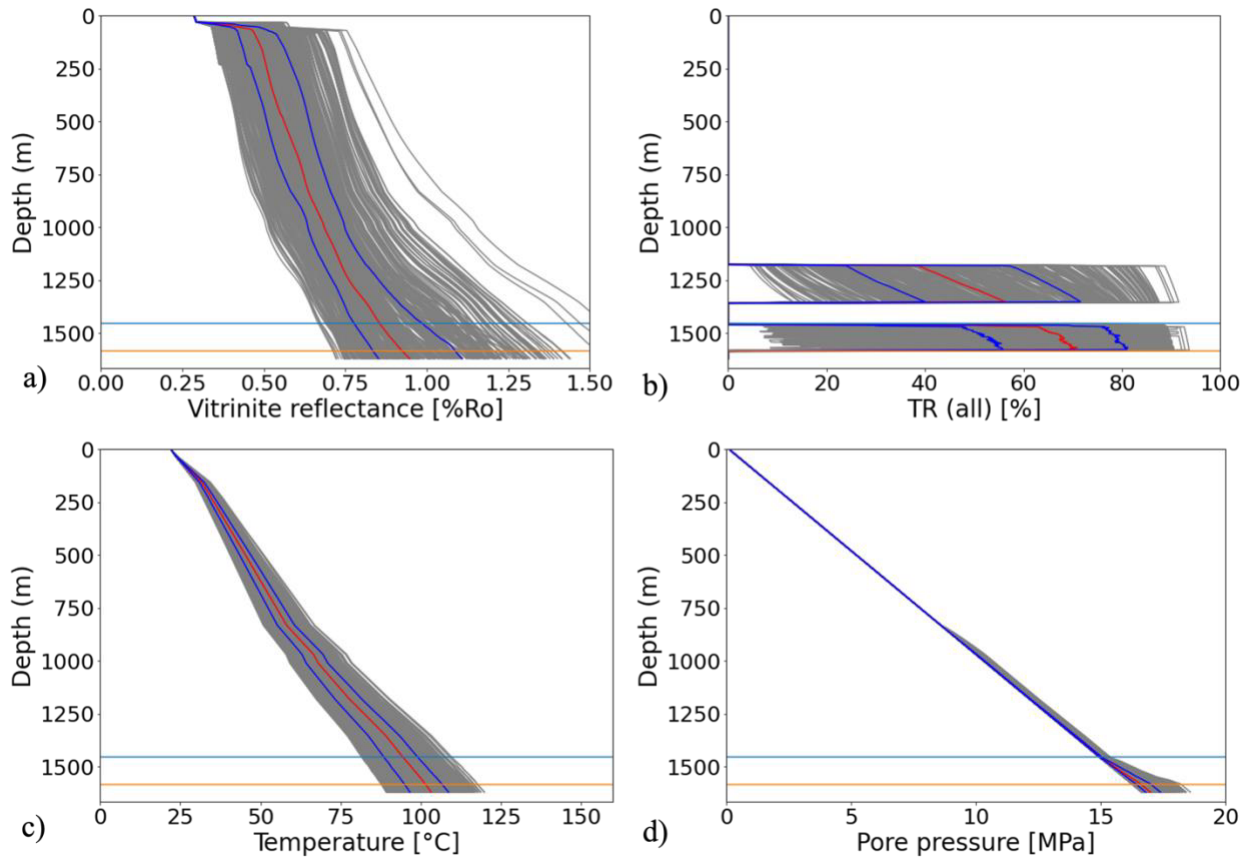


Figure 11. Monte Carlo simulations of vitrinite reflectance (thermal maturity), transformation ratio (TR), temperature, and pore pressure. The grey curves represent individual realizations from the basin model simulations. The dark blue curves indicate the 25th and 75th percentiles, while the red curves show the median. The light blue and light orange curves represent the top and bottom boundaries of the Goldwyer III Formation, respectively.

6.3 Uncertainty reduction

One of the key advantages of the Monte Carlo basin modeling approach is its ability to reduce the uncertainty in thermal maturity estimates by incorporating uncertainty of geological history, petrological inputs, and physical constraints. To evaluate this, we compare vitrinite reflectance estimated from three different methods: (1) Monte Carlo basin modeling in this study; (2) rock physics inversion which estimates maturity based on present-day petrophysical and seismic signatures (Huang et al., 2025); (3) T_{\max} -based empirical calculation, which uses geochemical measurements to estimate vitrinite reflectance (Jarvie, 2001).

Figure 12 shows that all the T_{\max} -derived vitrinite reflectance values fall within the range of realizations from the Monte Carlo basin modeling and most of the values lie within the interquartile range of the simulation results, indicating strong agreement. The distribution plot further illustrates that the posterior distribution of vitrinite reflectance from the rock physics inversion shows limited updating with respect to its prior, while the distribution from the Monte Carlo basin modeling is narrower and closely aligns with the calculated vitrinite reflectance values. This reduction in uncertainty reflects the additional geological constraints introduced by the forward modeling

process that incorporates the geohistory of the basin in addition to rock physics and seismic signatures.

These results demonstrate that Monte Carlo basin modeling improves confidence in thermal maturity predictions, which is a significant advantage for hydrocarbon generation assessments and risk reduction in exploration.

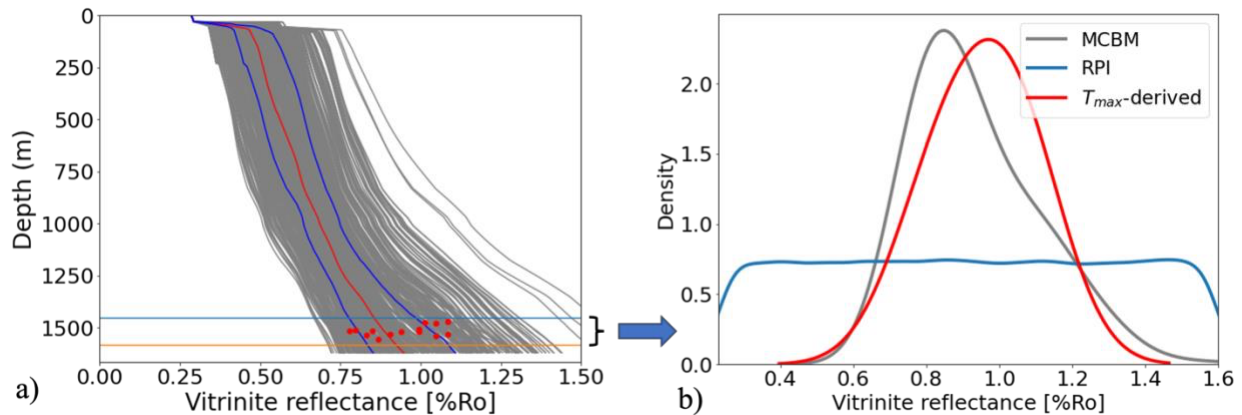


Figure 12. Comparison of vitrinite reflectance from different sources. a). Monte Carlo basin modeling and T_{max} -derived vitrinite reflectance. The grey curves represent individual realizations from the basin model simulations. The dark blue curves indicate the 25th and 75th percentiles, while the red curves show the median. The light blue and light orange curves represent the top and bottom boundaries of the Goldwyer III Formation, respectively. The red dots are the T_{max} -derived vitrinite reflectance. b). Distributions of vitrinite reflectance within the Goldwyer III Formation from Monte Carlo basin modeling (grey curve), posterior of rock physics inversion (blue curve), and T_{max} -based calculation (red curve).

7 Conclusion

This study presents a comprehensive Monte Carlo basin modeling framework that can incorporate uncertainties in petrological inputs, paleo-erosion magnitudes, organic facies properties, and boundary conditions to quantify key source rock properties, including vitrinite reflectance, transformation ratio, temperature, and pore pressure.

The simulation results show that the source rock within the Goldwyer III Formation in the study area is in the oil or wet gas window with substantial but incomplete transformation.

Sensitivity analysis indicates that Cretaceous erosion and heat flow are the dominant factors influencing thermal maturity. The transformation ratio also shows strong sensitivity to the hydrocarbon generation kinetic model, highlighting the importance of selecting appropriate kinetic parameters when evaluating hydrocarbon generation potential.

A comparison of thermal maturity results from Monte Carlo basin modeling, rock physics inversion, and T_{max}-based empirical methods demonstrates that the Monte Carlo approach significantly reduces uncertainty. The basin modeling outputs not only align well with

geochemical maturity indicators but also exhibit narrower distributions compared to rock physics inversion, reflecting the added value of incorporating geological and physical constraints.

Despite these strengths, there are several limitations in this study. Firstly, there are no calibration data such as borehole temperature and lab measured vitrinite reflectance. Incorporating such data in future studies could further reduce uncertainty in source rock property estimates. Second, although the Monte Carlo framework allows for comprehensive uncertainty quantification, the overall workflow remains computationally intensive. While the simulation itself runs efficiently, performance bottlenecks occur during the editing, saving, and loading of lithology configurations and output files. Further optimization is needed to improve data handling efficiency and streamline the modeling process. Third, the current implementation uses 1D basin models. Extending the approach to 2D or 3D models in future work could better capture spatial heterogeneity and improve the accuracy and reliability of the results, at more computational cost.

Overall, this integrated framework improves the robustness and reliability of source rock property predictions and provides a valuable workflow for source rock evaluation, risk assessment, and decision-making in hydrocarbon exploration.

Acknowledgement

This work is supported by the funding from the sponsors of the Stanford Center for Earth Resources Forecasting (SCERF) and Stanford Natural Gas Initiative (NGI). We thank Western Australia's Department of Mines, Industry Regulations and Safety for providing the necessary data used in this study. We would also like to acknowledge Lukman Mobolaji Johnson from University of Ilorin for his thoughtful discussion.

Reference

Al Ibrahim, M. (2019). *Petroleum system modeling of heterogeneous organic-rich mudrocks*. Stanford University. GitHub site: : <https://github.com/MosGeo/BPSMAutoToolbox>

Allen, P. A., & Allen, J. R. (2005). *Basin analysis: Principles and applications* (2nd ed.). Blackwell Publishing.

Allen, P. A., & Allen, J. R. (2013). *Basin analysis: Principles and application to petroleum play assessment*. John Wiley & Sons.

Athy, L. F. (1930). Density, porosity, and compaction of sedimentary rocks. *Aapg Bulletin*, 14(1), 1-24.

Brevik*, I., Szydluk, T., Corver, M. P., De Prisco, G., Stadler, C., & Helgesen, H. K. (2014). Geophysical basin modeling: Generation of high quality velocity and density cubes for seismic imaging and gravity field monitoring in complex geology settings. In *SEG Technical Program Expanded Abstracts 2014* (pp. 4733-4737). Society of Exploration Geophysicists.

Cadman, S., Pain, L., Vuckovic, V., & Le Poidevin, S. (1993). *Canning Basin* (Vol. 9). Australian Petroleum Accumulations Report, Western Australia, 81 pp.

D'Ercole, C., Gibbons, L., & Ghorji, K. A. R. (2003). *Prospects and leads, central Canning Basin, Western Australia, 2003* (Record 2003/14). Western Australia Geological Survey.

Fenwick, D., Scheidt, C., & Caers, J. (2014). Quantifying asymmetric parameter interactions in sensitivity analysis: application to reservoir modeling. *Mathematical Geosciences*, 46, 493-511.

Finder Exploration. (2018). Maturity and unconventional resource modelling: April 2018 update for Finder Exploration's Pan-Canning Goldwyer unconventional limit project (PC-GULP) [PowerPoint slides]. Finder Exploration. (<https://wapims.dmp.wa.gov.au/WAPIMS/>)

Fonseca, J., Pradhan, A., & Mukerji, T. (2023). Bayesian geophysical basin modeling with seismic kinematic metrics to quantify uncertainty for pore pressure prediction. *Geophysics*, 88(6), M239-M259.

Foster, C. B., O'Brien, G. W., & Watson, S. T. (1986). Hydrocarbon source potential of the Goldwyer Formation, Barbwire terrace, Canning basin, western Australia. *The APPEA Journal*, 26(1), 142-155.

Ghorji, K. A. R., & Haines, P. W. (2007). Paleozoic petroleum systems of the Canning Basin, Western Australia: a review. *Search and Discovery*, 5.

Haines, P. W. (2004). *Depositional facies and regional correlations of the Ordovician Goldwyer and Nita Formations, Canning Basin, Western Australia, with implications for petroleum exploration* (Record 7). Geological Survey of Western Australia.

Haines, P. W. (2011). Geology, exploration history, and petroleum prospectivity of state acreage release area L11-5, Canning Basin, Western Australia. *Perth: Geological Survey of Western Australia*, 1-10.

Hantschel, T., & Kauerauf, A. I. (2009). *Fundamentals of basin and petroleum systems modeling*. Springer Science & Business Media.

Hsu, C. S., & Robinson, P. R. (Eds.). (2017). *Springer handbook of petroleum technology*. Springer.

Huang, J., Scheirer, A. H., & Mukerji, T. (2025). Statistical rock physics inversion for assessing source rock potentials from seismic signatures: An application to the Canning Basin, Australia. *EarthArXiv*. <https://doi.org/10.31223/X5R15G>

Iqbal, M. A., Rezaee, R., Laukamp, C., Pejčić, B., & Smith, G. (2022). Integrated sedimentary and high-resolution mineralogical characterisation of Ordovician shale from Canning Basin, Western Australia: Implications for facies heterogeneity evaluation. *Journal of Petroleum Science and Engineering*, 208, 109347.

Jarvie, D. M., Claxton, B. L., Henk, F., & Breyer, J. T. (2001, June). Oil and shale gas from the Barnett Shale, Fort Worth basin, Texas. In *AAPG annual meeting program* (Vol. 10, p. A100).

Johnson, L. M. (2019). *Integrated Reservoir Characterization of the Goldwyer Formation Canning Basin* (Doctoral dissertation, Curtin University).

Johnson, L. M., Rezaee, R., Kadkhodaie, A., Smith, G., & Yu, H. (2017). A new approach for estimating the amount of eroded sediments, a case study from the Canning Basin, Western Australia. *Journal of Petroleum Science and Engineering*, 156, 19-28.

Johnson, L. M., Rezaee, R., Smith, G. C., Mahlstedt, N., Edwards, D. S., Kadkhodaie, A., & Yu, H. (2020). Kinetics of hydrocarbon generation from the marine Ordovician Goldwyer Formation, Canning Basin, Western Australia. *International Journal of Coal Geology*, 232, 103623.

Kibria, M. G., Das, S., Hu, Q. H., Basu, A. R., Hu, W. X., & Mandal, S. (2020). Thermal maturity evaluation using Raman spectroscopy for oil shale samples of USA: comparisons with vitrinite reflectance and pyrolysis methods. *Petroleum Science*, 17, 567-581.

MacKay, D. J. (2003). *Information theory, inference and learning algorithms*. Cambridge university press.

Minka, T. (2000). *Estimating a Dirichlet distribution*.

Norris, J. R. (1998). *Markov chains* (No. 2). Cambridge university press.

Park, J., Yang, G., Satija, A., Scheidt, C., & Caers, J. (2016). DGSA: A Matlab toolbox for distance-based generalized sensitivity analysis of geoscientific computer experiments. *Computers & geosciences*, 97, 15-29.

Pepper, A. S., & Corvi, P. J. (1995). Simple kinetic models of petroleum formation. Part I: oil and gas generation from kerogen. *Marine and petroleum geology*, 12(3), 291-319.

Peters, K. E., & Cassa, M. R. (1994). *Applied source rock geochemistry*.

Peters, K. E., Curry, D. J., & Kacwicz, M. (2012). An overview of basin and petroleum system modeling: Definitions and concepts.

Schenk, C. J., Tennyson, M. E., Mercier, T. J., Woodall, C. A., Finn, T. M., Le, P. A., ... & Leathers-Miller, H. M. (2018). *Assessment of undiscovered oil and gas resources in the Canning Basin Province, Australia, 2017* (No. 2018-3023). US Geological Survey.

Sweeney, J. J., & Burnham, A. K. (1990). Evaluation of a simple model of vitrinite reflectance based on chemical kinetics. *AAPG bulletin*, 74(10), 1559-1570.

Tipsword, H. L., Setzer, F. M., & Smith Jr, F. L. (1966). Interpretation of depositional environment in Gulf Coast petroleum exploration from paleoecology and related stratigraphy.

Tong, Y., & Mukerji, T. (2017). Generalized sensitivity analysis study in basin and petroleum system modeling, case study on Piceance Basin, Colorado. *Journal of Petroleum Science and Engineering*, 149, 772-781.

Tømmerås, A., Sylta, Ø., Daszinnies, M. C., & Mencaroni, D. (2018). Prewell and postwell predictions of oil and gas columns using an iterative Monte Carlo technique with three-dimensional petroleum systems modeling. *AAPG Bulletin*, 102(4), 709-728.

Virtanen, P., Gommers, R., Oliphant, T. E., Haberland, M., Reddy, T., Cournapeau, D., ... & Van Mulbregt, P. (2020). SciPy 1.0: fundamental algorithms for scientific computing in Python. *Nature methods*, 17(3), 261-272.

Young, A., Flament, N., Hall, L., & Merdith, A. (2021). The influence of mantle flow on intracontinental basins: Three examples from Australia. *Basin Research*, 33(2), 1429-1453.

Wygrala, B. P. (1989). Integrated study of an oil field in the southern Po basin, northern Italy.

Young, A., Flament, N., Hall, L., & Merdith, A. (2021). The influence of mantle flow on intracontinental basins: Three examples from Australia. *Basin Research*, 33(2), 1429-1453.